SAND2000-3115J

# Statistical Properties of Antenna Impedance in an Electrically Large Cavity*

Larry K. Warne, Kelvin S. H. Lee, H. Gerald Hudson,
William A. Johnson, Roy E. Jorgenson, and Stephen L. Stronach†

December 8, 2000

**Abstract**

This paper presents models and measurements of antenna input impedance in resonant cavities at high frequencies. The behavior of input impedance is useful in determining the transmission and reception characteristics of an antenna (as well as the transmission characteristics of certain apertures). Results are presented for both the case where the cavity is undermoded (modes with separate and discrete spectra) as well as the overmoded case (modes with overlapping spectra). A modal series is constructed and analyzed to determine the impedance statistical distribution. Both electrically small as well as electrically longer resonant and wall mounted antennas are analyzed. Measurements in a large mode stirred chamber cavity are compared with calculations. Finally a method based on power arguments is given, yielding simple formulas for the impedance distribution.

## 1 INTRODUCTION

This paper constructs models for the input impedance $Z_{in}$ of linear antennas in an electrically large cavity [1]. Cases where modes have overlapping spectra, and the antenna impedance approaches the free space value [2], as well as separate discrete spectra [3], [4] are both considered in this statistical treatment. The behavior of the impedance and its extreme values are useful in determining the transmission and reception characteristics of an antenna (as well as the transmission characteristics of certain apertures) and practical bounds for these quantities. An electrically short center driven dipole is treated first by means of a modal series for the cavity field. The statistical properties of this high-frequency cavity field are introduced from which distributions for the impedance are extracted by means of Monte Carlo simulation and asymptotic analysis. These are compared to measurements in a mode stirred chamber. It is then shown how these results apply to an electrically longer resonant dipole and a wall-mounted monopole antenna. The known enhancement of the field near the cavity wall is shown to correspond to the behavior of the field correlation function, which is used in the treatment of the monopole antenna. Finally, a simplified approach using conservation of power is carried out that yields practically useful formulas for the impedance distributions and extreme values.

*Sandia is a multiprogram laboratory operated by Sandia Corporation, a Lockheed Martin Company, for the United States Department of Energy under Contract DE-AC04-94AL85000.

†The authors are with Sandia National Laboratories, Albuquerque, NM, except Dr. Lee who is with ITT Industries/AES, Los Angeles, CA.

## 2 ELECTRICALLY SHORT ANTENNA

Using a modal series for the cavity field [4], [5], with time dependence $e^{-i\omega t}$, the input impedance of an electrically short dipole aligned with the $z$ axis is

$$Z_{in} \sim R - iX + R_{rad} \sum_n \left(\frac{2\pi Q}{k^3 V}\right) \frac{\left(i\omega^2/Q\right)\omega^2/\omega_n^2}{\omega^2\left(1+i/Q\right)-\omega_n^2} 3A_{nz}^2\left(\underline{r}\right) \tag{1}$$

where $R_{rad}$ is the antenna radiation resistance in free space, which for a short dipole of length $2h$, with triangular current distribution, is [6]

$$R_{rad} \sim \frac{\eta_0}{6\pi}\left(kh\right)^2 \tag{2}$$

The quantity $\eta_0 \approx 120\pi$ ohms is the impedance of free space and $k = \omega/c$ is the wavenumber ($c$ is the vacuum velocity of light). The quantity $Z = R - iX$ is the local impedance of the antenna, consisting of the ohmic resistance $R$ and local reactance $X$ (this includes the quasistatic part of the cavity summation), which is approximately capacitive $1/\left(\omega C\right)$ for a short dipole [6]

$$C \sim \frac{2\pi\varepsilon_0 h}{\Omega_e} \tag{3}$$

where the expansion parameter is

$$\Omega_e = \Omega - 2\left(1+\ln 2\right) \tag{4}$$

the antenna fatness parameter is $\Omega = 2\ln\left(2h/a\right)$, and $a$ is the dipole radius. The cavity volume is $V$, its quality factor is $Q$, and the cavity vector potential eigenfunctions are $\underline{A}_n$, normalized such that [4]

$$\frac{1}{V}\int_V \underline{A}_n \cdot \underline{A}_n dV = 1 \tag{5}$$

## 3 STATISTICS OF CAVITY FIELD

This paper is concerned with electrically large, complex cavities, for which a statistical description of the modes in (1) becomes applicable [7], [8], [9], [10], [11]. The cavity eigenvalues (resonant frequencies) $\omega_n$ have spacings that can be described by a slowly varying mean $\langle\Delta\omega_n\rangle$ times a random variable $s$

$$\Delta\omega_n = \omega_{n+1} - \omega_n = \langle\Delta\omega_n\rangle s \tag{6}$$

where the asymptotic formula for the mean is [12], [13]

$$\langle\Delta\omega_n\rangle \sim \pi^2 c^3/\left(V\omega_n^2\right)\ ,\ \omega_n \to \infty \tag{7}$$

The probability density function for the normalized spacing $s$ is Poisson (exponential) when the cavity geometry is simple (e.g., separable, where eigenvalue degeneracy occurs frequently) [11], [12]

## DISCLAIMER

This report was prepared as an account of work sponsored by an agency of the United States Government. Neither the United States Government nor any agency thereof, nor any of their employees, make any warranty, express or implied, or assumes any legal liability or responsibility for the accuracy, completeness, or usefulness of any information, apparatus, product, or process disclosed, or represents that its use would not infringe privately owned rights. Reference herein to any specific commercial product, process, or service by trade name, trademark, manufacturer, or otherwise does not necessarily constitute or imply its endorsement, recommendation, or favoring by the United States Government or any agency thereof. The views and opinions of authors expressed herein do not necessarily state or reflect those of the United States Government or any agency thereof.

## DISCLAIMER

Portions of this document may be illegible in electronic image products. Images are produced from the best available original document.

RECEIVED
DEC 22 2000
OSTI

$$f_s^P(s) = e^{-s}, \, 0 < s < \infty \tag{8}$$

and is Rayleigh (Wigner) when the cavity is complex [10], [12]

$$f_s^W(s) = \frac{\pi}{2} s e^{-s^2 \pi/4}, \, 0 < s < \infty \tag{9}$$

Complex geometry is typical of applications and thus the Rayleigh spacing is more frequently encountered. Constant spacing

$$s \equiv 1 \tag{10}$$

is also useful to study because it gives similar results for the impedance as does the Rayleigh spacing, but is simple enough that asymptotic analysis of the modal series can be carried out.

The cavity eigenfunctions are taken to be isotropic (all three components have similar statistics) with Gaussian density [7], [11]

$$\zeta = \sqrt{3} A_{nz} \tag{11}$$

$$f_\zeta(\zeta) = \frac{1}{\sqrt{2\pi}} e^{-\zeta^2/2} \tag{12}$$

which follows the chosen normalization [7]

$$3 \int_{-\infty}^{\infty} A_{nz}^2 f_{A_{nz}}(A_{nz}) \, dA_{nz} = \int_{-\infty}^{\infty} \zeta^2 f_\zeta(\zeta) \, d\zeta = 1 \tag{13}$$

An argument in support of the Gaussian nature of the eigenfunctions, relates to the ray description of these eigenfunctions, where the ray contributions to the modal field at an observation point consist of many separate returns from the complex cavity boundary that are uncorrelated [11], [7]. Experiments on cavities with smooth walls have shown that deviations from this simple density do arise and can be included as contributions corresponding to periodic ray trajectories [11], [14], [15].

The correlation function for the eigenfunction components is different than that for scalar wavefunctions [11] and is given by [2], [16]

$$\rho_z(z_1, z_2) = \frac{\langle A_{nz}(z_1) A_{nz}(z_2) \rangle}{\sqrt{\langle A_{nz}^2(z_1) \rangle \langle A_{nz}^2(z_2) \rangle}} = \frac{3}{2} \left( 1 + \frac{1}{k_n^2} \frac{\partial^2}{\partial z_1^2} \right) \frac{\sin[k_n(z_1 - z_2)]}{k_n(z_1 - z_2)} \tag{14}$$

where $k_n = \omega_n / c$.

# 4 EXPERIMENTS AND SIMULATIONS

The parameter that describes the degree of spectral overlap is

$$\alpha = k^3 V / (2\pi Q) \tag{15}$$

This parameter is the ratio of the energy stored in the cavity modes over a narrow spectral bandwidth (containing many complete modes) to the same energy if the modal amplitudes are fixed at the average peak level. If the cavity is undermoded (separate discrete modal spectra) $\alpha << 1$. If the cavity is overmoded (many overlapping modes) $\alpha >> 1$. Figures 1 through 3 show Smith charts for the input impedance of near resonant monopoles in the wall of a mode stirred chamber for the undermoded through overmoded range.

The mode stirred chamber (37 ft x 23 ft x 13 ft) has a volume of $V \approx 313$ m$^3$. The cavity is not simply a rectangular box, since a mode stirrer was present in the chamber, but was not moved during the frequency sweeps that generated the data. The quality factor of the chamber was determined to be $Q \approx 80,000$ by examining the 3 dB width of isolated modes at 220 MHz; at 920 MHz it was estimated from the 220 MHz value, by the scaling $\sqrt{\omega}$, to be approximately $Q \approx 165,000$; at 15 GHz it was taken as the experimental value $1,280,000$. The antennas were near resonant wall mounted monopoles. The dimensions of the monopoles were $2a \approx 0.102$ in, $h \approx 12.953$ in at 220 MHz, $h \approx 2.97$ in at 920 MHz, and $2a \approx 1.51$ mm with $h \approx 4.325$ mm at 15 GHz.

Figures 4 and 5 illustrate the behavior of the spectra for the two limits of $\alpha$. Figures 6 and 7 show comparisons of the monopole input resistance with Monte Carlo simulation of the series

$$z_{in} = r_{in} - i x_{in} = (Z_{in} - Z) / R_{rad} \approx \left(\frac{2\pi Q}{k^3 V}\right) \sum_{n_r} \frac{i\omega / (2Q)}{\omega (1 + i/(2Q)) - \omega_n} 3 A_{nz}^2 (\underline{r}) \tag{16}$$

where we have approximated the summand ($Q$ and $\langle \Delta\omega_n \rangle$ are approximated as constant also) since we are including only those modes near the observation range of $\omega$ values captured in the figures (the range of included modes $n_r$ contains a range of $\omega_n$ that is slightly larger than the $\omega$ range so that negligible error is incurred in this approximation). The simulations were done with all three types of eigenvalue spacings. The agreement with the experimental results is good; although there is some small variation with realization of the random numbers, the Rayleigh and uniform spacing results are in slightly better agreement with measurements than the Poisson spacing.

The near resonant monopoles in the experiment had nearly zero free space reactance (except the 920 MHz antenna which had the experimentally determined value $j8.5$ ohms). The experimentally determined free space value of the radiation resistances were 44 ohms at 220 MHz and 46 ohms at 920 MHz. The frequency span was 10 MHz with 4800 frequency points in the 220 MHz experiment; the simulations used 200 modes with 1000 frequency points. The frequency span was 1 MHz with 801 frequency points in the 920 MHz experiment; the simulations used 400 modes with 1000 frequency points. The frequency span was 10 MHz also with 801 frequency points in the 15 GHz experiment.

# 5 ASYMPTOTIC BEHAVIORS

Using the modal series it can be shown that the frequency average (taken over a narrow band, but including many complete modal spectra) of the normalized input impedance approaches unity [1]

$$\langle z_{in} \rangle_\omega = \frac{1}{\omega_+ - \omega_-} \int_{\omega_-}^{\omega_+} z_{in} d\omega \to 1 \tag{17}$$

It can also be shown in the overmoded limit that by replacing the modal sum by an integral (inserting $d\omega_n / \langle \Delta\omega_n \rangle$ in the summand) the impedance approaches unity [1]

$$z_{in} \to 1\,,\ \alpha \to \infty \tag{18}$$

In the next two subsections the uniformly spaced modal series is used to estimate extreme behaviors of the impedance.

## 5.1 Uniform Spacing, Single Mode

The undermoded limit $\alpha << 1$ has separated, discrete, spectra. The largest values of the input resistance and reactance in this region occur when $\omega$ is near a resonance. Thus we can consider a single mode of the series (the closest mode to the observation frequency) and estimate the extreme statistics by regarding $\omega - \omega_n$ to be a random variable with uniform density between $\pm \langle \Delta\omega_n \rangle / 2$ (for typically used uniform frequency sampling). The distribution function, derived from the ratio of independent random variables [17], for this case is

$$F(r_{in}) = 1 - \int_{r_{in}}^{\infty} f(r)\, dr \sim 1 + \frac{\alpha}{\pi}\sqrt{r_{in}\alpha/(2\pi)}\, e^{-r_{in}\alpha/4}\left[K_0(r_{in}\alpha/4) - K_1(r_{in}\alpha/4)\right],\ r_{in} >> \alpha,\ \alpha << 1 \tag{19}$$

where the identity [18] $\int_0^\infty e^{-\nu x}\frac{dx}{\sqrt{x(x+a)}} = e^{\nu a/2} K_0(\nu a/2)$ has been used and $K_0(x)$, $K_1(x)$ are the modified Bessel functions. Figures 8 and 9 show this result (long dashed curves) compared to measurements and Monte Carlo simulations of the uniformly spaced modal series ($\alpha$ is too large in Figure 9 for this result to be valid over any substantial range of $r_{in}$). Over most of the valid range (19) can be simplified to

$$F(r_{in}) \approx 1 - \frac{2}{\pi}\sqrt{\frac{2\alpha}{\pi r_{in}}},\ 1/\alpha >> r_{in} >> \alpha \tag{20}$$

However near the upper limit of $r_{in}$, the corresponding density function exhibits exponential behavior that allows one to establish practical upper bounds for the resistance values

$$f(r_{in}) \approx \frac{e^{-r_{in}\alpha/2}}{\pi r_{in}}\alpha,\ r_{in}\alpha >> 1 \tag{21}$$

The normalized reactance also exhibits exponential behavior near the upper limit (an averaging method [19] can be used to give a more uniformly valid expression) [1]

$$f(x_{in}) \approx \frac{\alpha\sqrt{2}}{\pi |x_{in}|} e^{-|x_{in}|\alpha},\ |x_{in}|\,\alpha >> 1 \tag{22}$$

which shows the extreme reactance magnitude is approximately half the extreme resistance.

The number of independent samples in a frequency sweep is dependent on the number of modes spanned. For example at 220 MHz there are only 141 modes in the frequency sweep even though there are many more frequencies sampled. If, for $\alpha << 1$, the frequency sweep is sufficiently fine to resolve the spectral peaks (over-sampling in frequency) then the density function of the peaks is of interest. Thus, near the upper limit

of $r_{in}$ we can set $\omega = \omega_n$ and find the single mode density function for the peak values (the square of a Gaussian random variable)

$$f(r_{in}) \approx \sqrt{\frac{\alpha}{2\pi r_{in}}} e^{-r_{in}\alpha/2}, \; r_{in}\alpha >> 1 \tag{23}$$

The exponential behavior in (23) is the same as (21). The distribution function corresponding to (23) is

$$F(r_{in}) \approx \operatorname{erf}\left(\sqrt{r_{in}\alpha/2}\right) \tag{24}$$

where $\operatorname{erf}(x)$ is the error function, and the number of independent samples corresponds to the number of modes contained in the frequency sweep.

## 5.2 Uniform Spacing, Between Modes

The smallest values of the input resistance for $\alpha << 1$ occur when $\omega$ is between modes. Taking the frequency to be exactly between modes of the uniformly spaced series, the modal terms can be taken in pairs about the observation frequency, each pair having a simple exponential distribution. The infinite summation requires an infinite sequence of convolutions to be performed to obtain the density function [17]. Using the Laplace transform to convert the convolutions to an infinite product, and using the identity [20] $\prod_{k=1}^{\infty}\left[1-\frac{x^2}{k^2-a^2}\right] = \frac{a}{\sqrt{a^2+x^2}}\frac{\sin\left(\pi\sqrt{a^2+x^2}\right)}{\sin(\pi a)}$ to evaluate the product, the density can be found by inverse transform of the resulting function for frequency samples between modes. The integral of the density function is thus the distribution

$$F(r_{in}) = F_\chi\left(\frac{\pi^2 r_{in}}{8\alpha}\right) \tag{25}$$

where from the residue method

$$F_\chi(\chi) = 1 - e^{-\chi 4\alpha^2/\pi^2}\cosh(\alpha)\frac{4}{\pi}\sum_{m=0}^{\infty}(-1)^m\frac{2m+1}{(2m+1)^2+4\alpha^2/\pi^2}e^{-(2m+1)^2\chi} \tag{26}$$

An alternative representation for the density function, that converges rapidly for $\chi \to 0$, can also be obtained from the inverse transform using the identity [21] $\frac{a}{2\sqrt{\pi t^3}}e^{-a^2/(4t)} = \frac{1}{2\pi i}\int_{c-i\infty}^{c+i\infty} e^{st}e^{-a\sqrt{s}}ds$ (although it is difficult to integrate to obtain the distribution function) $f(r_{in}) = f_\chi\left(\pi^2 r_{in}/(8\alpha)\right)\pi^2/(8\alpha)$

$$f_\chi(\chi) = e^{-\chi 4\alpha^2/\pi^2}\cosh(\alpha)\sqrt{\frac{\pi}{\chi^3}}\sum_{m=0}^{\infty}(-1)^m(m+1/2)\,e^{-(m+1/2)^2\pi^2/(4\chi)} \tag{27}$$

Figures 8 and 9 show this distribution function (short dashed curves) compared to measurements and Monte Carlo Simulations (this result describes the entire distribution in Figure 9 since the placement of $\omega$ is not critical when the modes are overlapping and $\alpha$ is of order unity).

Using the second representation (27) we see that the density function exhibits exponential decay for very small $r_{in}$

$$f(r_{in}) \sim \cosh(\alpha)\sqrt{\frac{2\alpha}{\pi r_{in}^3}}e^{-\alpha(r_{in}+1/r_{in})/2}, \; r_{in} << \alpha \tag{28}$$

which again allows one to establish practical lower bounds for the input resistance. For $\alpha << 1$, the $\alpha r_{in}/2$ term in the exponential can be dropped, and (28) can be integrated to give the distribution function $F(r_{in}) \approx 2\text{erfc}\left[\sqrt{\alpha/(2r_{in})}\right]$, where erfc$(x)$ is the complementary error function. The number of independent samples, when we are over-samping in frequency, is again the number of modes spanned in the frequency sweep.

For $\alpha$ of order unity, the first representation (26) can be used to give

$$f(r_{in}) \sim \frac{\pi}{2\alpha}\cosh(\alpha)\, e^{-r_{in}[(2\alpha)/\pi+\pi/(2\alpha)]\pi/4}\,,\; r_{in} \to \infty\,,\; \alpha = O(1) \tag{29}$$

showing the exponential decay for large $r_{in}$. If we take the overmoded limit $\alpha >> 1$, from the second representation (28) we find that the normalized input resistance is Gaussian distributed about the mean of unity

$$f(\rho_r) \sim \sqrt{\frac{\alpha}{2\pi}}e^{-\alpha\rho_r^2/2}\,,\; r_{in} = 1+\rho_r\,,\; \alpha \to \infty \tag{30}$$

### 5.3 Overmoded Limit

By the central limit theorem [17] we expect both components of the impedance to become Gaussian distributed in the overmoded limit $\alpha >> 1$ since many modes are equally contributing to the modal series. Finding the variance of both components thus allows us to write

$$z_{in} \sim 1 + r_0\zeta - ix_0\zeta'\,,\; \alpha >> 1 \tag{31}$$

where $\zeta$ and $\zeta'$ are independent, normalized, zero mean Gaussians, and the standard deviations are found to be [1]

$$r_0 = x_0 = 1/\sqrt{\alpha} \tag{32}$$

## 6 ELECTRICALLY LONGER ANTENNA

The preceding analytical and simulation results were based on the assumption of an electrically short dipole, but the experiments were conducted using near resonant monopole antennas. This conflicting situation will be resolved in the present and next sections. The integro-differential equation for a center driven linear antenna inside a cavity can be written as

$$-V_0\delta(z) = E_z \approx$$

$$-\frac{i\omega}{\varepsilon_0 V}\sum_n \frac{\omega^2(1+i/Q)/\omega_n^2}{\omega^2(1+i/Q)-\omega_n^2}A_{nz}(z)\int_{-h}^{h}A_{nz}(z')\,I(z')\,dz' + \frac{i\omega\mu_0}{4\pi}\left[\left(1+\frac{1}{k^2}\frac{\partial^2}{\partial z^2}\right)\int_{-h}^{h}\frac{I(z')\,dz'}{\sqrt{a^2+(z-z')^2}} - I(z)\right] \tag{33}$$

where the second term is the local quasistatic contribution. The antenna current distribution $I(z)$ is the unknown. The antenna is assumed to be thin and thus the local quasistatic term can be thought of as having the transmission line form

$$\left(1+\frac{1}{k^2}\frac{\partial^2}{\partial z^2}\right)\int_{-h}^{h}\frac{I(z')\,dz'}{\sqrt{a^2+(z-z')^2}}\approx\Omega_e\left(1+\frac{1}{k^2}\frac{\partial^2}{\partial z^2}\right)I(z) \tag{34}$$

This term, in addition to the boundary conditions

$$I(\pm h)=0 \tag{35}$$

play a dominant role in determining the distribution of current (at least up to the first resonance). The leading term of the current can thus be taken as

$$I(z)\approx I_0\sin k(h-|z|) \tag{36}$$

The impedance is then found by using this current, and the integro-differential representation for the electric field (33), in the stationary (first order corrections to the current do not contribute) EMF representation [6]

$$Z_{in}=-\frac{1}{I^2(0)}\int_V \underline{E}\cdot\underline{J}dV \tag{37}$$

Noting that the integral of a Gaussian random process is a Gaussian random variable [17] we find

$$Z_{in}\approx R-iX+\sum_n\left(\frac{\eta_0k^2}{2\pi}U_n^{tot}\right)\left(\frac{2\pi Q}{k^3V}\right)\frac{(i\omega^2/Q)\,\omega^2/\omega_n^2}{\omega^2(1+i/Q)-\omega_n^2}3A_{nz}^2 \tag{38}$$

where again the antenna ohmic resistance is $R$ and the local reactance is (we are ignoring quasistatic images in the cavity walls)

$$X\approx-\frac{\eta_0}{2\pi}\Omega_e\cot(kh)$$

$$+\frac{\eta_0}{2\pi}\frac{1}{\sin^2(kh)}\left[2\,\mathrm{Si}(kh)+\sin(2kh)\left\{2\mathrm{Cin}(kh)-\mathrm{Cin}(2kh)-\frac{3}{4}\right\}-\cos(2kh)\left\{\mathrm{Si}(2kh)-2\,\mathrm{Si}(kh)\right\}-\frac{1}{2}kh\right] \tag{39}$$

and $\mathrm{Si}(x)$, $\mathrm{Cin}(x)$ are the sine and cosine integrals. The variance of the stochastic integral appearing in the impedance representation (37) is

$$U_n^{tot}=\frac{1}{\sin^2(kh)}\int_{-h}^{h}\sin k(h-|z|)\int_{-h}^{h}\frac{3}{2}\left(1+\frac{1}{k_n^2}\frac{\partial^2}{\partial z^2}\right)\frac{\sin k_n(z-z')}{k_n(z-z')}\sin k(h-|z'|)\,dz'dz \tag{40}$$

A small error is made (mostly in the reactance) if we set $k_n\to k$ in $U_n^{tot}$ for all values of $\alpha$ (this approximation is consistent with the previously discussed truncation of the series in the range of the resonant modes). If $k_n$ is retained in $U_n^{tot}$, it can be shown in the overmoded limit $\alpha >> 1$, that the correct total antenna reactance [6] $X_{in}=-\frac{\eta_0}{2\pi}\Omega_e\cot(kh)+\frac{\eta_0}{4\pi}\left[2\,\mathrm{Si}(2kh)+\sin(2kh)\left\{-2+2\mathrm{Cin}(2kh)-\mathrm{Cin}(4kh)\right\}\right.$

$-\cos(2kh)\{\mathrm{Si}(4kh) - 2\,\mathrm{Si}(2kh)\}]/\sin^2(kh)$ is produced rather than the value $X$, that is obtained when the approximation $k_n \to k$ is invoked; at low frequencies these expressions become the same; even for $kh = \pi/2$, where the dominant leading term of the reactance vanishes, the error is $X \approx 64$ ohms versus the correct $X_{in} \approx 43$ ohms. The result of the replacement $k_n \to k$ is

$$Z_{in} \approx R - iX + R_{rad} \sum_n \left(\frac{2\pi Q}{k^3 V}\right) \frac{(i\omega^2/Q)\,\omega^2/\omega_n^2}{\omega^2(1+i/Q) - \omega_n^2} 3A_{nz}^2 \tag{41}$$

surprisingly, the same result we had previously for the short antenna, except that the radiation resistance $R_{rad}$ is now the correct free space value for the electrically longer antenna [6], given by

$$(4\pi/\eta_0)\sin^2(kh)\,R_{rad} = 2\mathrm{Cin}(2kh) + \sin 2kh\,[\mathrm{Si}(4kh) - 2\mathrm{Si}(2kh)] - \cos 2kh\,[\mathrm{Cin}(4kh) - 2\mathrm{Cin}(2kh)] \tag{42}$$

Thus the quantity $z_{in} = (Z_{in} - Z)/R_{rad}$ from the electrically short antenna theory is approximately the same for electrically longer antennas.

# 7 MONOPOLE ANTENNA AND WALL BEHAVIOR

A previous paper [16] has shown that the correlation dyad for the field is proportional to the imaginary part of the dyadic Green's function. Thus in a local vicinity of the cavity boundary (near the wall mounted monopole antenna) at $z = 0$, we can use the half space dyadic Green's function to obtain the correlation function transition near the cavity wall. The result is

$$R_{zz}^h(z_1, z_2) = \frac{3}{2}\left(1 + \frac{1}{k_n^2}\frac{\partial^2}{\partial z_1^2}\right)\left[\frac{\sin k_n(z_1 - z_2)}{k_n(z_1 - z_2)} + \frac{\sin k_n(z_1 + z_2)}{k_n(z_1 + z_2)}\right] \tag{43}$$

Using this correlation function, it is easy to show [1] that the impedance of a wall-mounted monopole is half that of the dipole. Thus, again the quantity $z_{in} = (Z_{in} - Z)/R_{rad}$ for the monopole is the same as for the dipole (assuming $R_{rad}$ is taken to be the monopole free space radiation resistance), and the comparisons with experiment, made above, are justified.

It is interesting that the known 3 dB wall enhancement of the normal electric field [22], and its transition into the cavity volume are represented by this half space correlation function

$$\frac{\left\langle |E_{norm}|^2 \right\rangle}{\left\langle |E_i|^2 \right\rangle} = 1 + \frac{3}{2}\left(1 + \frac{\partial^2}{\partial u^2}\right)\frac{\sin u}{u}\bigg|_{u=2kz} = R_{zz}^h(z, z) \tag{44}$$

Figures 10 through 12 show a mode stirred chamber experiment and results verifying the presence of this wall enhancement in the undermoded region. The normal electric field distribution on the wall is 3 dB higher than in the volume of the cavity (this is borne out for the field as a function of frequency in Figure 11, and approximately for the field at the resonant mode frequencies in Figure 12).

# 8 POWER BALANCE

Now that the usefulness of the electrically short antenna theory has been demonstrated, we return to the electrically short antenna and develop a practically useful simplified model.

We break up the field at the antenna $E_z$ into the sum of a reflected part $E_z^{ref}$ and a part $E_z^{rad}$ radiated as if in free space. The impedance components of the short dipole are correspondingly broken into the sums

$$R_{in} = R_{rad} + R_{wall} \tag{45}$$

and

$$X_{in} = X + X_{wall} \tag{46}$$

The quantity $R_{rad}$ is the free space radiation resistance associated with the field $E_z^{rad}$ and $X$ is the local reactance associated with the quasistatic part of the field $E_z^{rad}$. The quantities $R_{wall}$ and $X_{wall}$ are associated with the reflected field from the cavity wall $E_z^{ref}$. The wall impedance $Z_{wall} = R_{wall} - iX_{wall}$ can be written in terms of the received voltage at the dipole due to the reflected field $V_{ref} \sim -hE_z^{ref}$

$$Z_{wall} = V_{ref}/I(0) = -hE_z^{ref}/I(0) = \frac{-E_z^{ref}}{\sqrt{\left\langle |E_z|^2 \right\rangle_V}} h\sqrt{U/(3\varepsilon_0/2)} \tag{47}$$

where the received voltage has been determined from the effective height (the positive reference of the voltage is on the positive $z$ arm of the antenna) of the short dipole, and the mean energy density in the cavity is

$$U = \frac{3}{2}\varepsilon_0 \left\langle |E_z|^2 \right\rangle_V \tag{48}$$

where the subscript $V$ denotes volume average. Now using the definition of cavity quality factor

$$Q = \frac{\omega V U}{P_{in}} \tag{49}$$

with the average power into the antenna (the dissipated power) given by

$$P_{in} = \frac{1}{2} R_{in} |I(0)|^2 \tag{50}$$

we obtain

$$Z_{wall} = \frac{-E_z^{ref}}{\sqrt{\left\langle |E_z|^2 \right\rangle_V}} \sqrt{\frac{Q h^2 R_{in} \eta_0}{3kV}} \tag{51}$$

Identifying the radiation resistance of a short dipole in free space $R_{rad}$ (2) in this expression, using the definition of $\alpha$ (15), and using lower case impedances to denote the quantities $r_{wall} = R_{wall}/R_{rad}$ and $x_{wall} = X_{wall}/R_{rad}$ (note that this scaled reactance is really the same as $x_{in}$, since $x_{in}$ was defined with the local reactance subtracted out), we finally obtain

$$r_{wall} = r_{in} - 1 = r\sqrt{r_{in}/\alpha} \tag{52}$$

$$x_{wall} = \zeta\sqrt{r_{in}/\alpha} \tag{53}$$

where

$$\tau = \frac{-\mathrm{Re}\left(E_z^{ref}\right)}{\sqrt{\left\langle |E_z|^2 \right\rangle_V}} \tag{54}$$

$$\zeta = \frac{\mathrm{Im}\left(E_z^{ref}\right)}{\sqrt{\left\langle |E_z|^2 \right\rangle_V}} \tag{55}$$

## 8.1 Extreme Values

The quantities $\tau$ and $\zeta$ in (52) and (53) describe the fluctuation of the real and imaginary parts of the reflected field at the antenna location normalized by the mean cavity field. For the present we assume $\tau$ and $\zeta$ have normalized Gaussian densities with zero mean (this assumption is refined in the next subsection). To obtain an extreme value curve for the impedance variation we could take these random variables to be fixed at, say, the three sigma point $M_0 = 3$ of the underlying real and imaginary Gaussian distributions. It is interesting to note that if the cavity field is viewed as **a three dimensional standing wave in the frequency range of the fundamental cavity modes, then the maximum-to-mean-ratio of the field is eight-to-one,** corresponding to the value $M_0 = 2\sqrt{2}$; a value that is **not very different from the three sigma value $M_0 = 3$; these extreme results may therefore be useful at lower frequencies than anticipated.** Replacing $\tau$ and $\zeta$ with this value and solving the quadratic equation gives

$$r_{in} = 1 + \frac{1}{2\alpha}M_0^2\cos^2\varphi \pm \sqrt{\left(1 + \frac{1}{2\alpha}M_0^2\cos^2\varphi\right)^2 - 1} \tag{56}$$

$$x_{wall} = \pm M_0 \sin\varphi\sqrt{r_{in}/\alpha} \tag{57}$$

The dashed circles in Figures 1 through 3 are plots of these results. These extreme circles provide a reasonable containment of the experimental impedance variations. The radiation resistance of the 15 GHz monopole was taken as the nominal 36 ohm value.

The extreme values of the real and imaginary parts on this circle can be easily found as

$$1 + \frac{1}{2\alpha}M_0^2 - \sqrt{\left(1 + \frac{1}{2\alpha}M_0^2\right)^2 - 1} < r_{in} < 1 + \frac{1}{2\alpha}M_0^2 + \sqrt{\left(1 + \frac{1}{2\alpha}M_0^2\right)^2 - 1} \tag{58}$$

$$|x_{wall}| < \sqrt{\left(1 + \frac{1}{2\alpha}M_0^2\right)^2 - 1} \tag{59}$$

The highly undermoded limit is $1/\left(2 + M_0^2/\alpha\right) < r_{in} < \left(2 + M_0^2/\alpha\right)$ and $2\,|x_{wall}| < 2 + M_0^2/\alpha$. The highly overmoded limit is $1 - M_0/\sqrt{\alpha} < r_{in} < 1 + M_0/\sqrt{\alpha}$ and $|x_{wall}| < M_0/\sqrt{\alpha}$, thus giving $r_{in} \to 1$ and $x_{wall} \to 0$.

## 8.2 Density

The distribution of input resistance generated by the power balance results, using the normalized Gaussian assumption for the normalized reflected field in (52), is shown as the dotted curves in Figures 13 and 14. The extreme values are representative but the midrange distribution is not even close to the experimental or simulation results. Using the modal series field representation we can generate the actual distributions for $\tau$ and $\zeta$, from which we construct more accurate density function approximations. Taking $I(0)$ to be real and positive (this choice is to be noted when interpreting the real and imaginary parts of the reflected field) we find

$$\frac{-E_z^{ref}}{\sqrt{\left\langle |E_z|^2 \right\rangle_V}} \approx i \frac{\sum_{n_r} \frac{3A_{nz}^2}{\pi(\omega-\omega_n)/\langle\Delta\omega_n\rangle+i\alpha}}{\sqrt{\sum_{n_r} \frac{3A_{nz}^2}{|\pi(\omega-\omega_n)/\langle\Delta\omega_n\rangle+i\alpha|^2}}} - \frac{1}{\sqrt{\sum_{n_r} \frac{3A_{nz}^2}{|\pi(\omega-\omega_n)/\langle\Delta\omega_n\rangle+i\alpha|^2}}} \tag{60}$$

The first term, which corresponds to the total normalized field at the antenna, has a positive real part. The second term, which corresponds to the normalized radiated field at the antenna, is negative real. Note that the local quasistatic normalized field has been subtracted from each term in the difference. In the undermoded limit $\alpha << 1$ the first term is imaginary except in the narrow frequency band about the resonances. The real part is thus skewed toward negative values. Thus we try taking the asymmetric Gaussian

$$f(\tau) \approx \frac{p(\alpha)}{\sqrt{2\pi}} e^{-\tau^2/2}, \; 0 < \tau < \infty$$

$$\approx \frac{2-p(\alpha)}{\sqrt{2\pi}} e^{-\tau^2/2}, \; -\infty < \tau < 0 \tag{61}$$

as a fit to the density function of the real part of the normalized scattered field. If we apply the result that $\langle r_{in}\rangle_\omega = \langle r_{in}\rangle_\tau \to 1$ we can determine the function of $\alpha$ as

$$p(\alpha) = 1 - 1/\left[2\sqrt{2\alpha/\pi} + e^{2\alpha}\mathrm{erfc}\left(\sqrt{2\alpha}\right)\right] \tag{62}$$

The function $p(\alpha)$ approaches $2\alpha$ as $\alpha \to 0$ and approaches 1 as $\alpha \to \infty$. Figures 15 and 16 show a comparison of the distributions for the real and imaginary parts of the normalized reflected field obtained from Monte Carlo simulations of the modal series representation (solid curves), and the asymmetric (short dashed curve) and symmetric (dotted curve) Gaussian distributions

$$F(\tau) \approx 1 - \frac{1}{2}p(\alpha)\,\mathrm{erfc}\left(\tau/\sqrt{2}\right), \; 0 < \tau < \infty$$

$$\approx \left[1 - \frac{1}{2}p(\alpha)\right]\mathrm{erfc}\left(-\tau/\sqrt{2}\right), \; -\infty < \tau < 0 \tag{63}$$

$$F(\zeta) = \frac{1}{2} + \frac{1}{2}\,\mathrm{erf}\left(\zeta/\sqrt{2}\right), \; -\infty < \zeta < \infty \tag{64}$$

Figure 15 used 500 modes; 100 modes at each end of the interval are beyond the sampled frequency range. Figure 16 used 1000 modes; 200 modes at each end of the interval are beyond the sampled frequency range. The agreement is reasonably good. The "kink" discrepancy in Figure 15 is caused by the discontinuity of the density function (61) at $\tau = 0$. The single mode approximate distribution $F(r_{in})$ (20) can be transformed by means of the quadratic relation $r_{in} = \left(\sqrt{\tau^2 + 4\alpha} + \tau\right)^2 / (4\alpha)$ to a distribution of normalized real scattered field, for small values of $\tau$ in the undermoded limit

$$F(\tau) \approx 1 - \frac{4\alpha}{\pi}\sqrt{\frac{2}{\pi}} / \left(\sqrt{\tau^2 + 4\alpha} + \tau\right), \; |\tau| << 1, \; \alpha << 1 \tag{65}$$

This simple approximate distribution indicates how the "kink" should be interpolated as shown by the long dashed curve in Figure 15. The short dashed curves in Figures 13 and 14 show the improvement in the power balance distributions by use of this asymmetric Gaussian distribution (representing the limited bandwidth of the resonances). The long dashed curve in Figure 13 shows the single mode approximate distribution (20) at the "kink" discrepancy.

The exponential decays of the density functions extracted in the asymptotic analyses are all reproduced by the power balance results. One might be tempted to use the asymmetrical Gaussian distribution (63) to refine the extreme curves (56) and (57), instead of basing these on the symmetrical three sigma point $M_0 = 3$. However, when the distributions are over-sampled in frequency, such that the resonances are fully resolved (for example the 220 MHz data), the extreme values must be determined from the confidence levels associated with the number of independent modes contained within the frequency sweep, as discussed in (24). Thus, the use of the symmetrical estimate, is appropriate for the extremes, when the data is over-sampled in frequency, but it is not appropriate for the midrange distribution.

# 9 CONCLUSIONS

The input impedance of linear antennas inside high $Q$, electrically large cavities, has been investigated theoretically and experimentally. Monte Carlo simulations based on a modal series representation, with statistical estimates for modal spacing and eigenfunction amplitudes, are found to agree with measurements in a mode stirred chamber cavity. The parameter $\alpha = k^3 V / (2\pi Q)$, equal to the ratio of modal width to modal spacing, determines the magnitude of the impedance variations; the undermoded limit (separated, distinct modal spectra) $\alpha << 1$ results in large variations; the overmoded limit (many overlapping modes) $\alpha >> 1$ results in small variations. Asymptotic analysis of the modal series yields formulas for the extreme values of the impedance. The modal series for an electrically short antenna has been shown to approximately represent resonant dipoles and wall mounted monopoles, provided the local impedance and free space radiation resistance parameters are appropriately modified; the half space correlation function used for the monopole treatment was shown to represent the known wall 3 dB normal field enhancement. A simplified model based on balance of power gives practically useful simple formulas for the impedance distributions and the extreme values.


# Acknowledgment

The authors would like to thank Kenneth C. Chen of Sandia National Laboratories for many helpful discussions on the power balance section and Ted H. Lehman for many helpful discussions regarding cavity mode statistics.

## References


[1] L. K. Warne, H. G. Hudson, W. A. Johnson, R. E. Jorgenson, S. L. Stronach of Sandia National Laboratories and K. S. H. Lee of ITT Industries/AES, *Input Impedance of Antennas in High Frequency Cavities*, Sandia Laboratories Report, SAND01-, January 2001.

[2] David A. Hill, *Linear Dipole Response in a Reverberation Chamber*, IEEE Transactions on Electromagnetic Compatibility, Vol. 41, No. 4, November 1999.

[3] Paul R. Berman (editor), **Cavity Quantum Electrodynamics**, Academic Press, Inc., Boston, 1994.

[4] William R. Smythe, **Static and Dynamic Electricity**, Hemisphere Pub. Corp., New York, 1989, Sections 13.30, 13.32, and 13.17.

[5] Robert E. Collin, **Field Theory of Guided Waves**, IEEE Press, New York, 1991, Sections 5.9 and 5.10.

[6] Edward C. Jordan and Keith G. Balmain, **Electromagnetic Waves and Radiating Systems**, Prentice-Hall, Inc., Englewood Cliffs, New Jersey, 1968, Sections 14.08, 14.09, 10.05, 10.07, 10.08, 14.05, and 14.06.

[7] T. H. Lehman, *A Statistical Theory of Electromagnetic Fields in Complex Cavities*, AFWL Interaction Note 494, May 1993.

[8] R. H. Price, H. T. Davis, and E. P. Wenaas, *Determination of the statistical distribution of electromagnetic-field amplitudes in complex cavities*, Physical Review E, vol. 48, No. 6, December 1993.

[9] Richard K. Chang and Anthony J. Campillo (editors), **Optical Processes in Microcavities**, World Scientific Pub. Co., New Jersey, 1996, pp389-426.

[10] Mandon Lal Mehta, **Random Matricies**, Academic Press, Inc., San Diego, 1991, Chapter 1.

[11] Martin C. Gutzwiller, **Chaos in Classical and Quantum Mechanics**, Springer-Verlag, Inc., New York, 1990, Chapter 16 (Sections 16.2, 16.3, 16.4, 16.7 ,16.8), Chapter 15 (Sections 15.5 and 15.6).

[12] S. Deus, P. M. Koch, and L. Sirko, *Statistical properties of the eigenfrequency distribution of three-dimensional microwave cavities*, Physical Review E., Vol. 52, No. 1, July 1995.

[13] R. Balian and C. Bloch, *Distribution of Eigenfrequencies for the Wave Equation in a Finite Domain. II. Electromagnetic Field. Riemannian Spaces*, Annals of Physics: 64, 271-307, 1971.

[14] L. E. Reichl, **The Transition to Chaos**, Springer-Verlag, Inc., New York, 1992, Chapter 8.

[15] Matthias Brack and Rajat K. Bhaduri, **Semiclassical Physics**, Addison Wesley Pub. Co., Reading Mass., 1997.

[16] L. K. Warne and K. S. H. Lee, *Some Remarks on Antenna Response in a Reverberation Chamber*, submitted to IEEE Transactions on Electromagnetic Compatibility.

[17] Athanasios Papoulis, **Probability, Random Variables, and Stochastic Processes**, McGraw-Hill Book Co., New York, 1965, pp. 126-127, 196-197, 189, 266-267, Sections 8-4, 14-1.

[18] I. S. Gradshteyn and I. M. Ryzhik, **Table of Integrals, Series, and Products**, Academic Press, New York, 1965, pp. 316.

[19] Kenneth C. Chen and Larry K. Warne, *Improved asymptotic expansions of time domain antenna current*, Radio Science, Vol. 26, No. 5, pp. 1205-1208, Sept.-Oct. 1991.

[20] L. B. W. Jolley, **Summation of Series**, Dover Pub., Inc., New York, 1961, pp. 196-197, 104.

[21] Milton Abramowitz and Irene A. Stegun, **Handbook of Mathematical Functions**, Dover Pub., Inc., New York, 1972, pp. 1026, 576.

[22] John M. Dunn, *Local, High-Frequency Analysis of the Fields in a Mode-Stirred Chamber*, IEEE Transactions on Electromagnetic Compatibility, Vol. 32, No. 1, Feb. 1990.

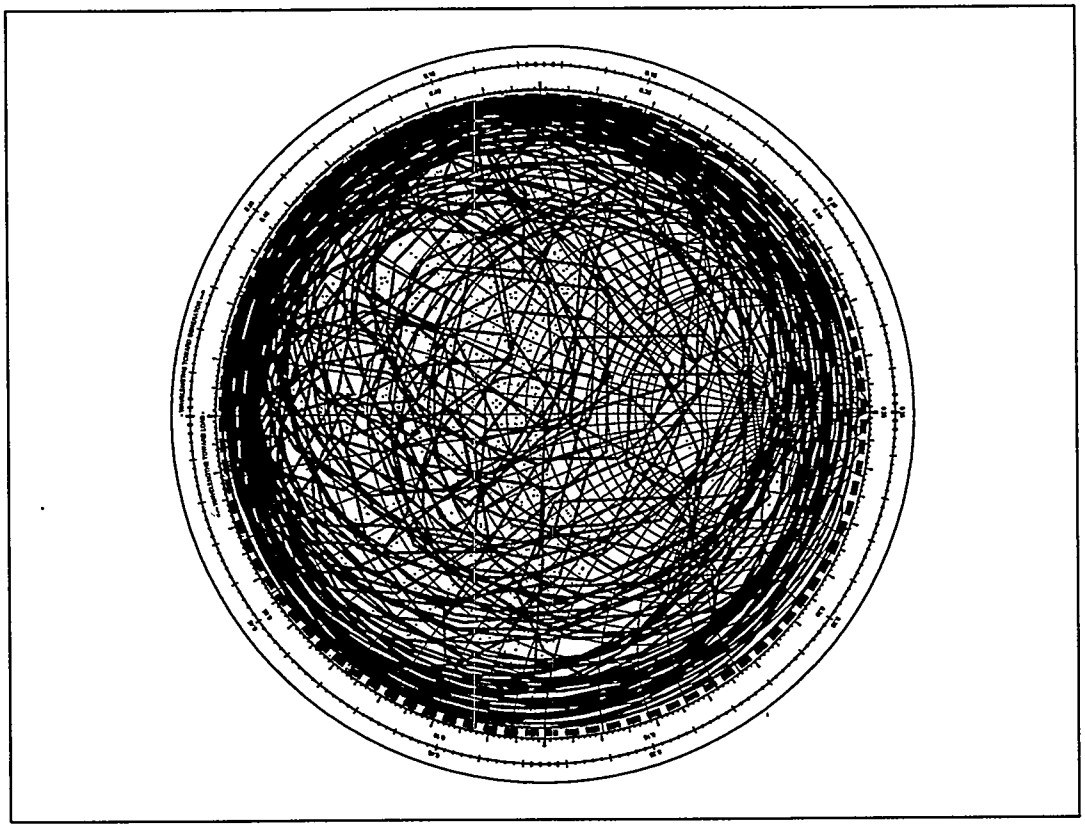

Figure 1: Fifty ohm Smith chart for input impedance of monopole at 220 MHz ($\alpha \approx 0.0609$) with 10 MHz sweep. "Bounding" power balance result comparison. Time dependence on the experimental Smith charts is $e^{j\omega t}$.

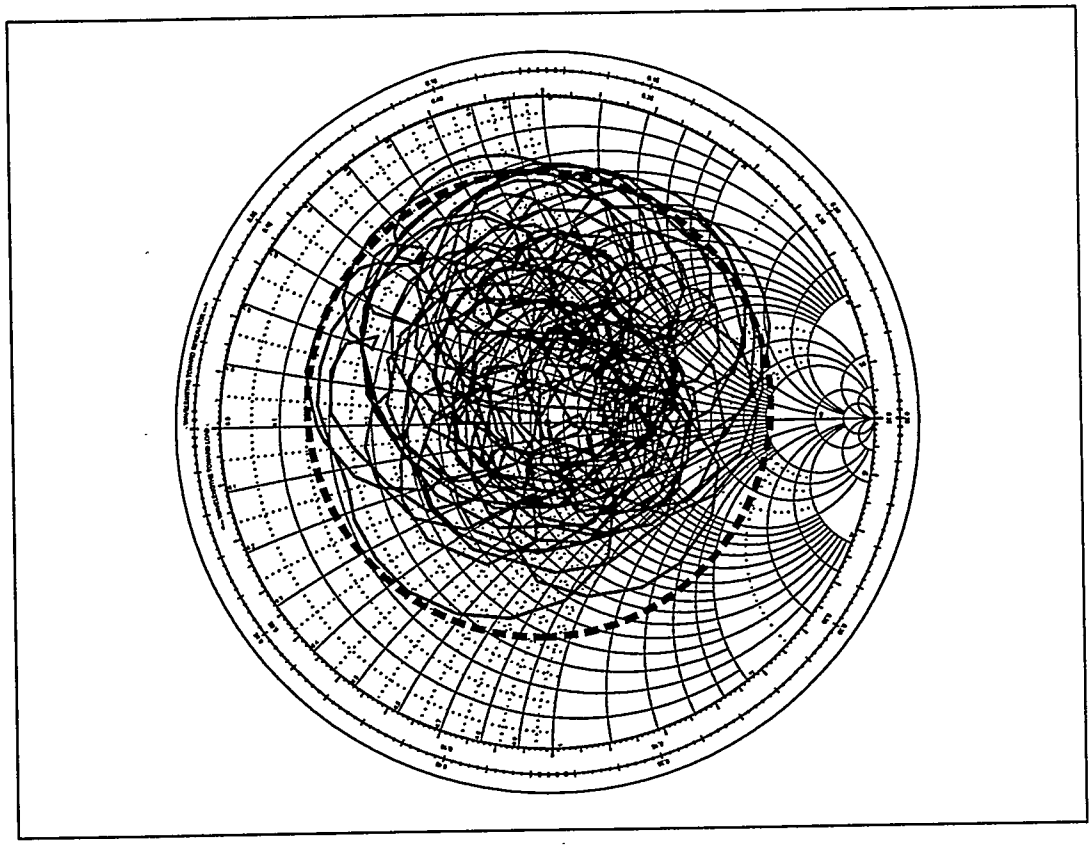

Figure 2: Fifty ohm Smith chart of input impedance of monopole at 920 MHz ($\alpha \approx 2.16$) with 1 MHz sweep. "Bounding" power balance result comparison.

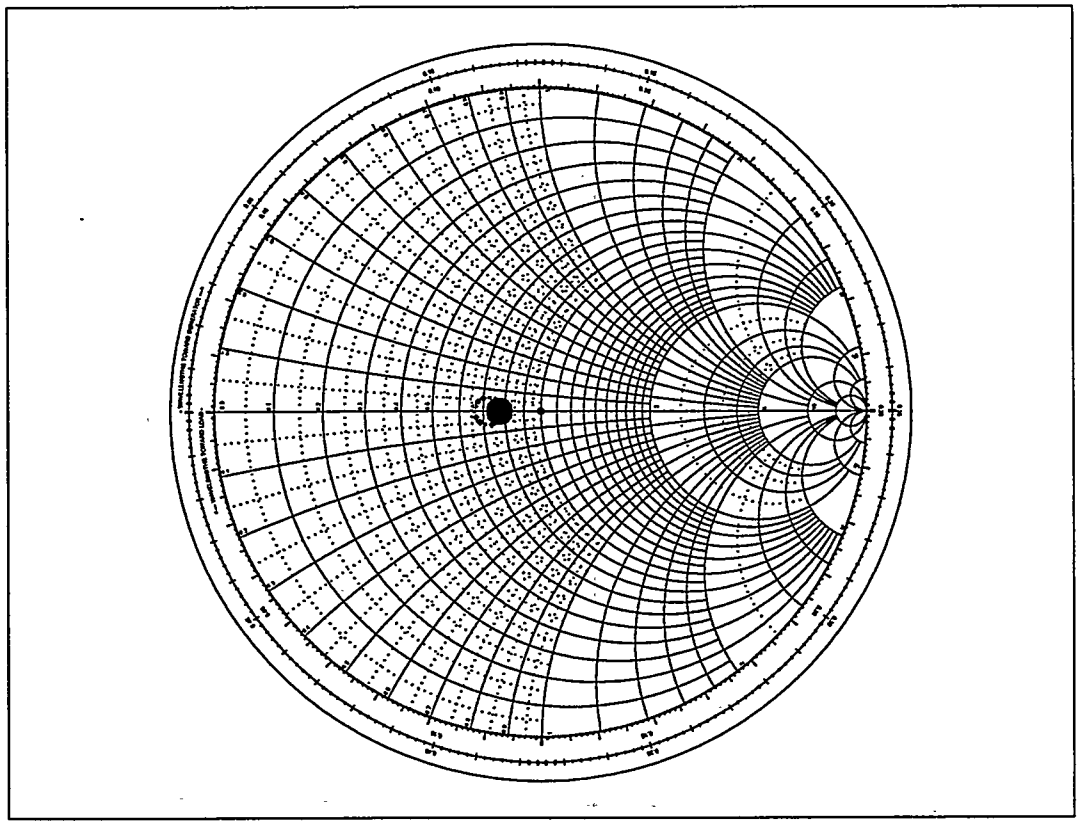

Figure 3: Fifty ohm Smith chart of input impedance of monopole at 15 GHz ($\alpha \approx 1206.7$) with 10 MHz sweep. "Bounding" power balance result comparison.

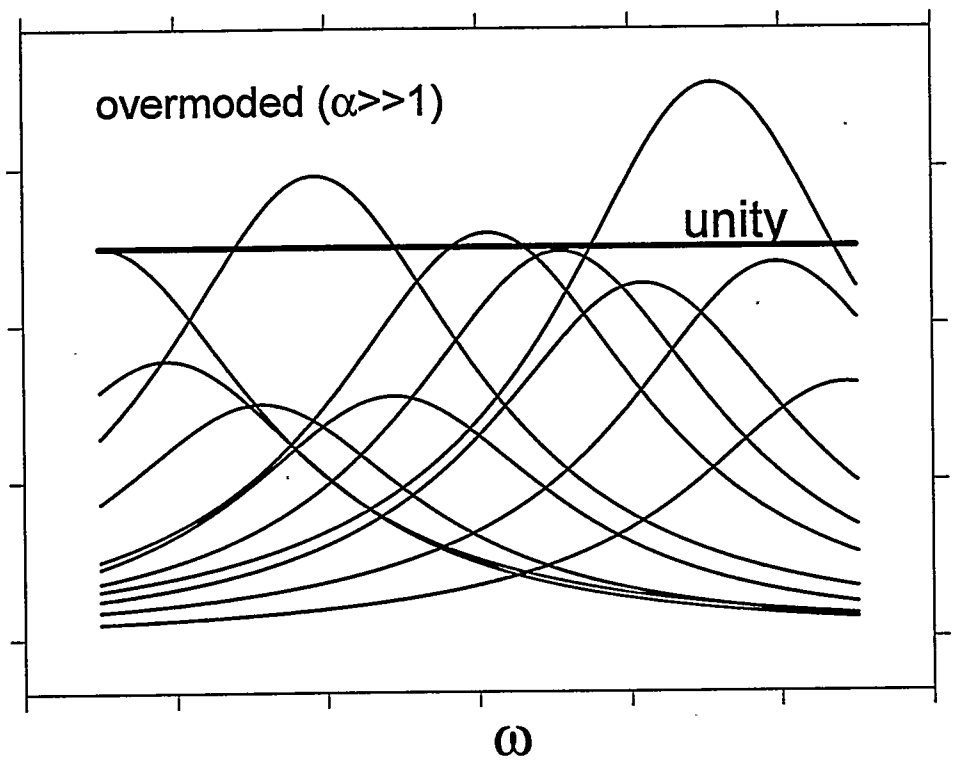


Figure 4: Energy spectra appearance when the cavity is overmoded $\alpha >> 1$.

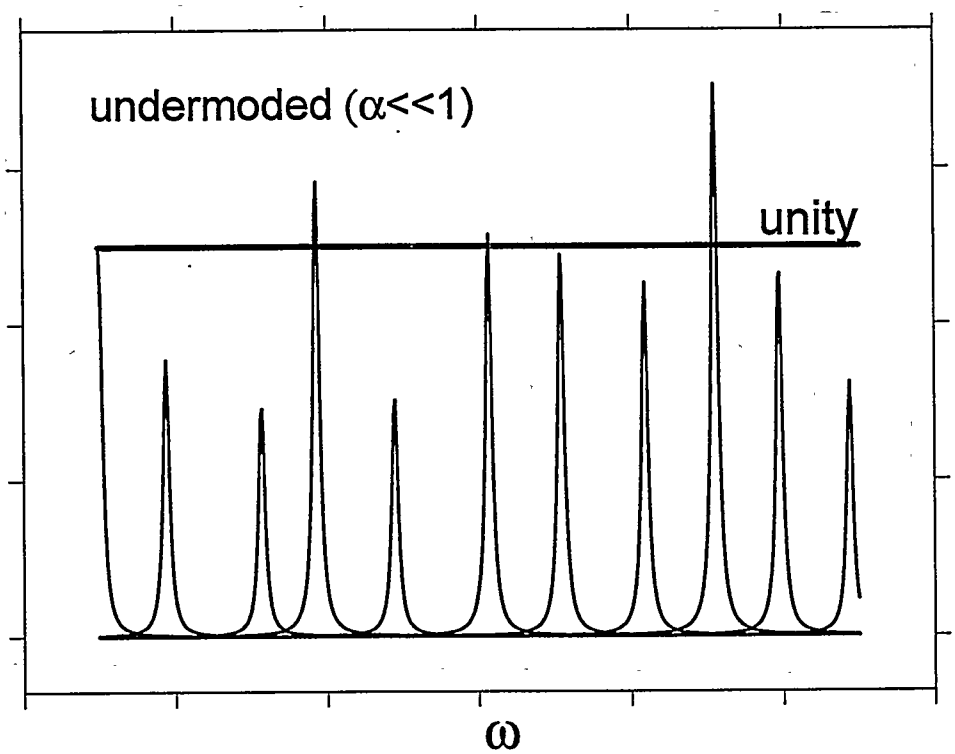


Figure 5: Energy spectra appearance when the cavity is undermoded $\alpha << 1$.

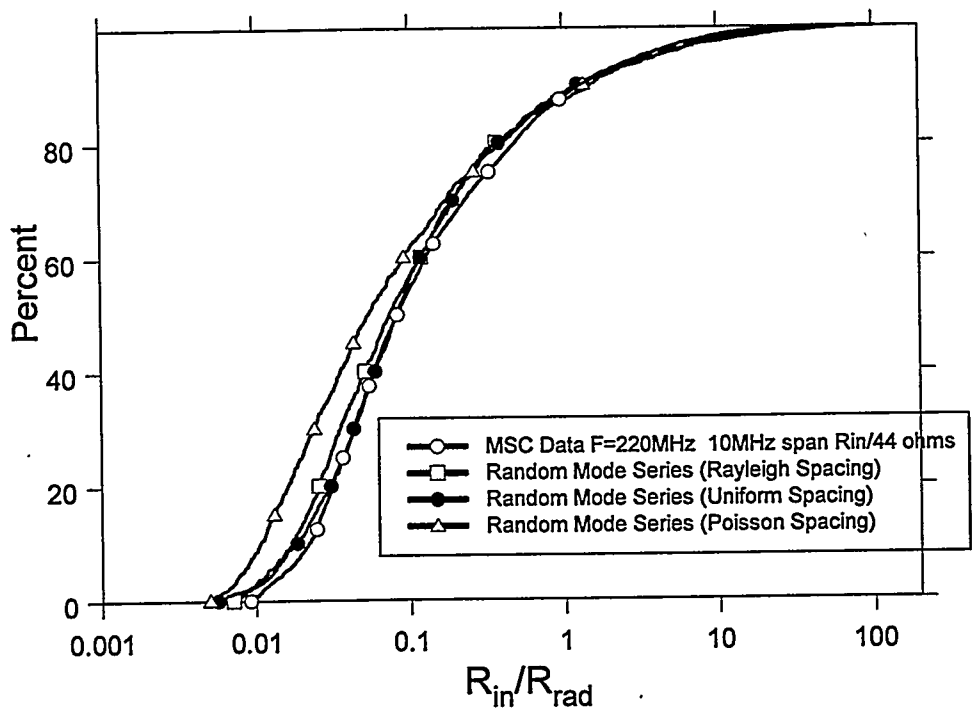


Figure 6: Normalized input resistance distribution from simulations and experiment at 220 MHz ($\alpha \approx 0.0609$).

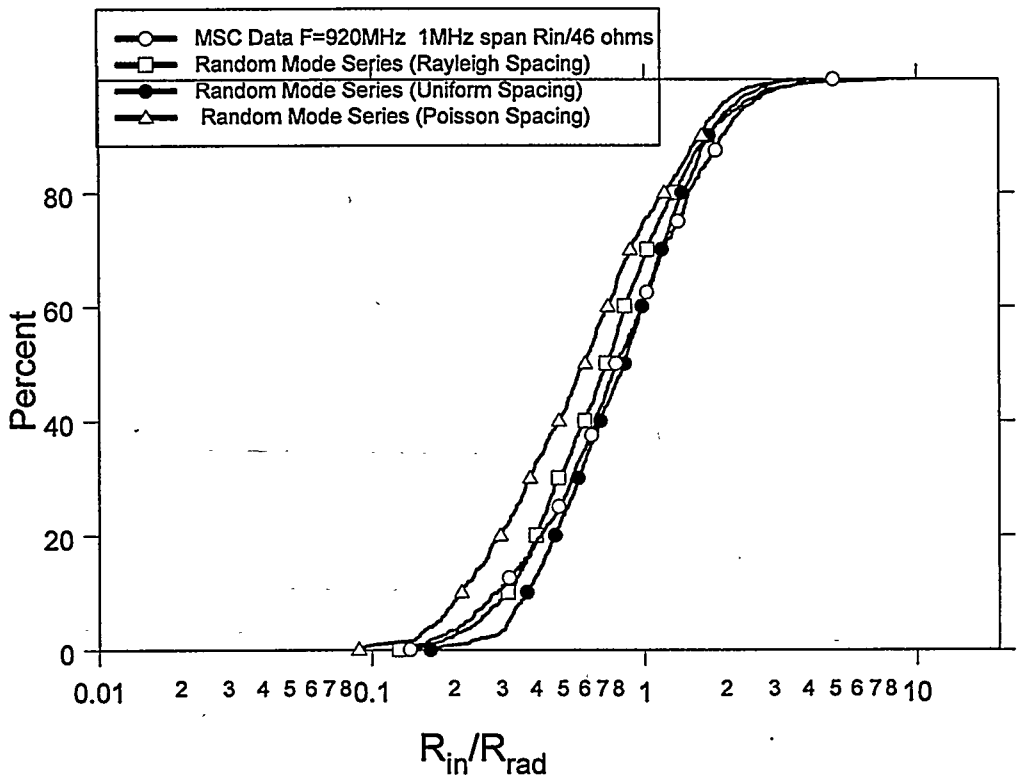


Figure 7: Normalized input resistance distribution from simulations and experiment at 920 MHz ($\alpha \approx 2.16$).

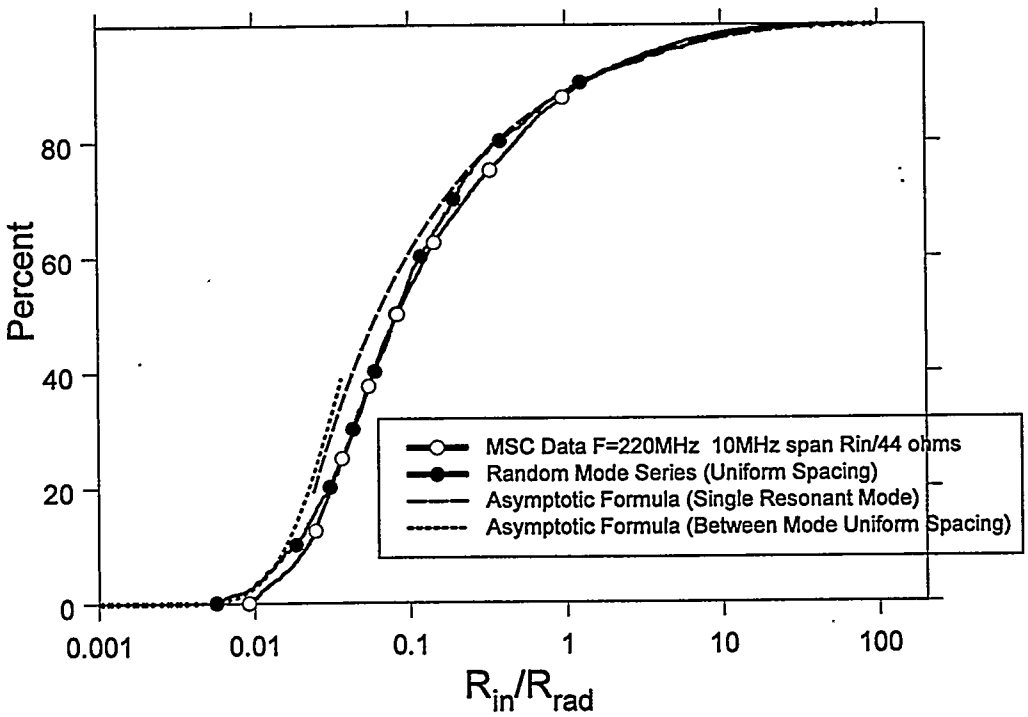


Figure 8: Comparison of asymptotic formulas, simulation, and experiment at 220 MHz with 10 MHz sweep.

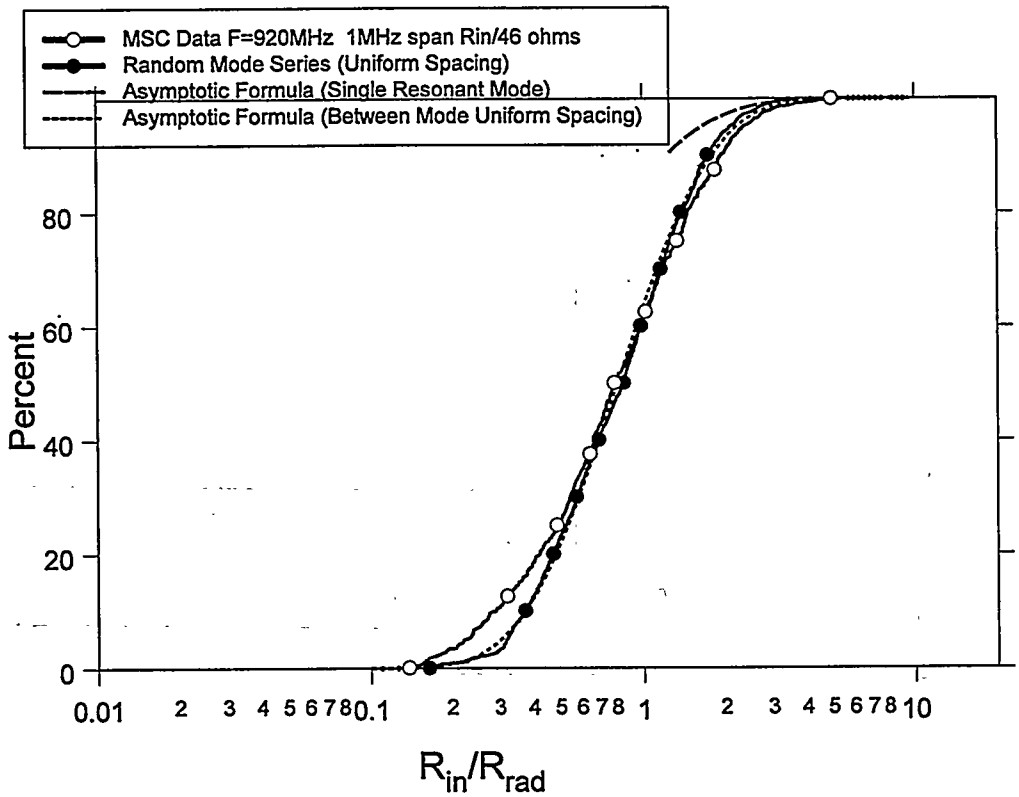


Figure 9: Comparison of asymptotic formulas, simulation, and experiment at 920 MHz with 1 MHz sweep.

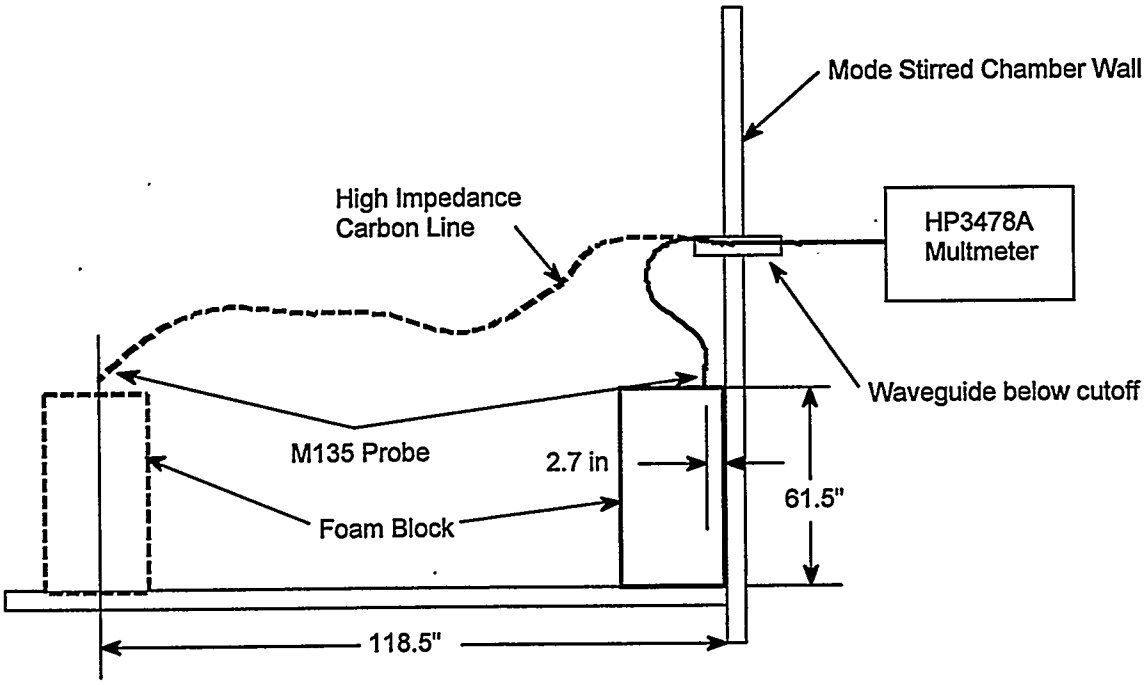


Figure 10: Drawing of 3 dB wall enhancement field measurement at 220 MHz using dipole probe.

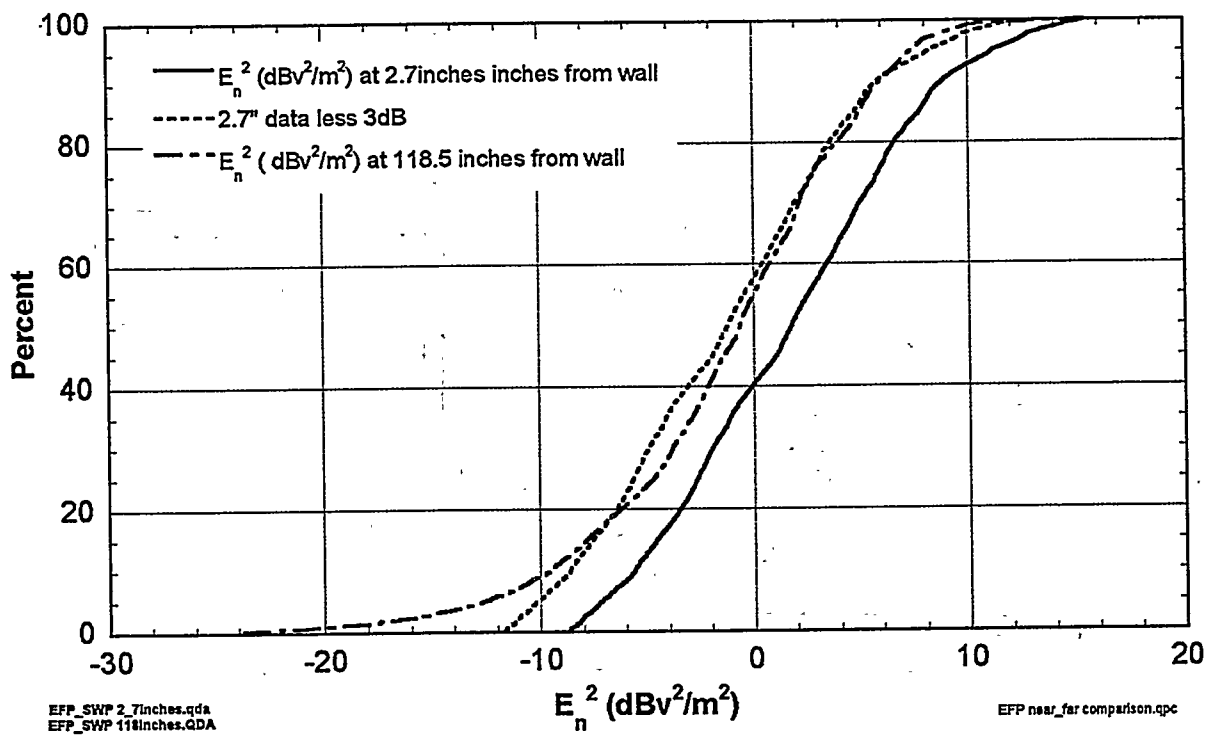


Figure 11: Electric field distribution from two dipole probes, one 2.7 inches from wall and one 118.5 inches from wall, showing 3 dB wall enhancement.

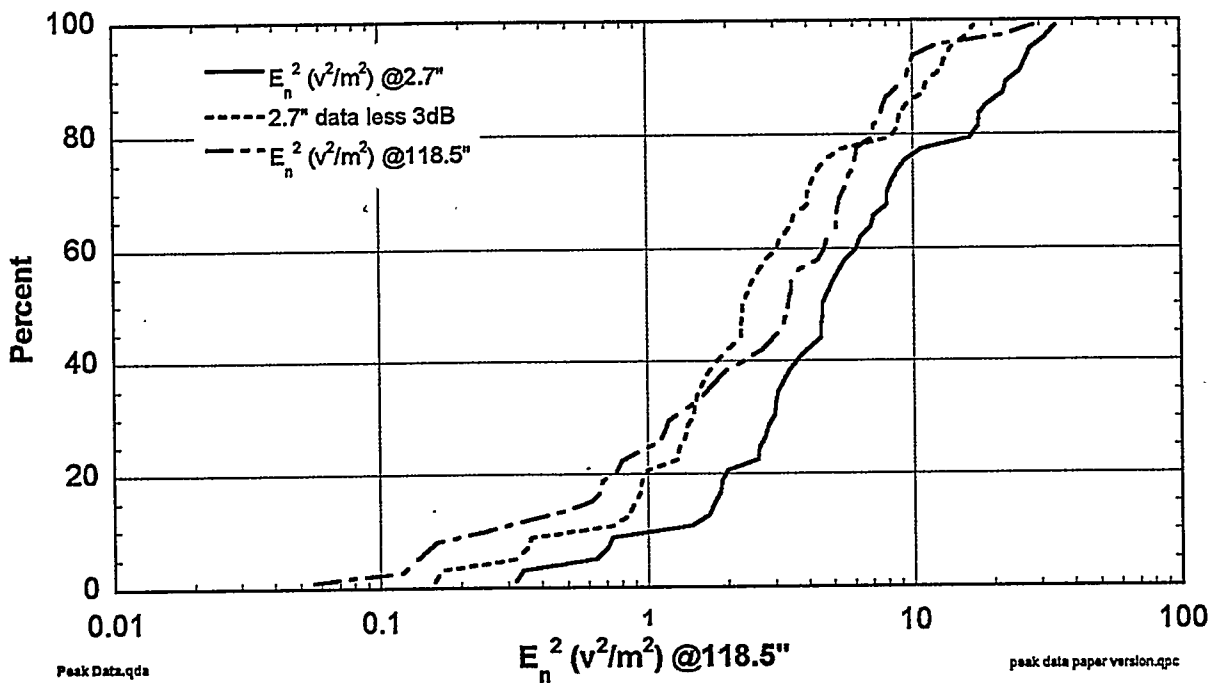


Figure 12: Electric field distribution from resonance peaks for both probes showing 3 dB wall enhancement.

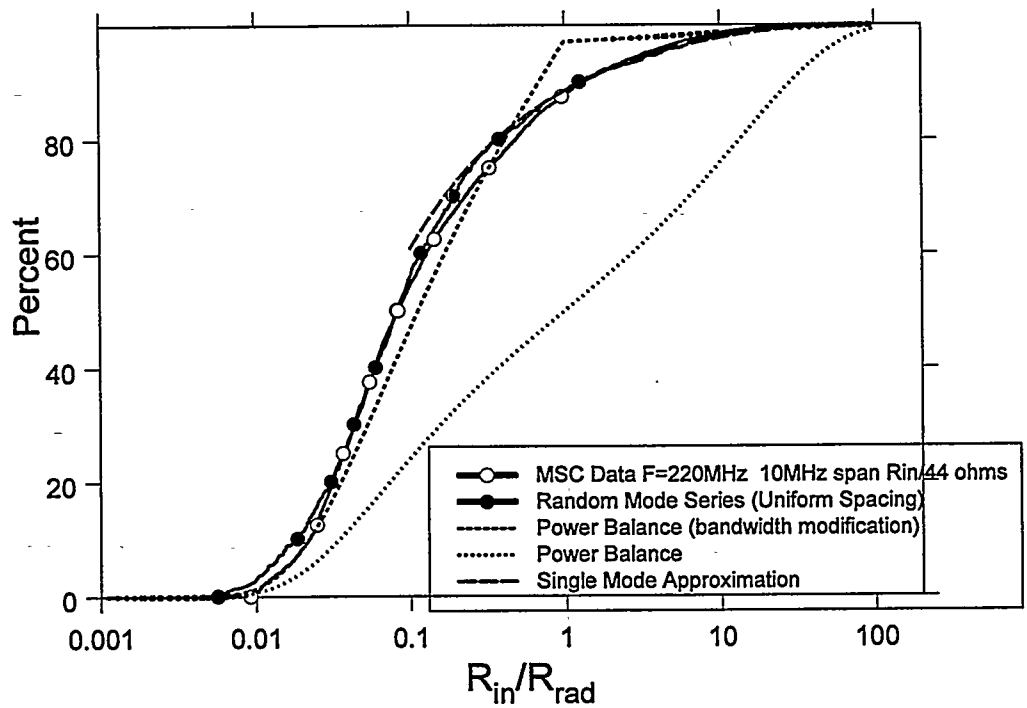


Figure 13: Normalized input resistance distribution from simulation, power balance (the bandwidth modification curve uses the asymmetric reflected field distribution) and experiment at 220 MHz.

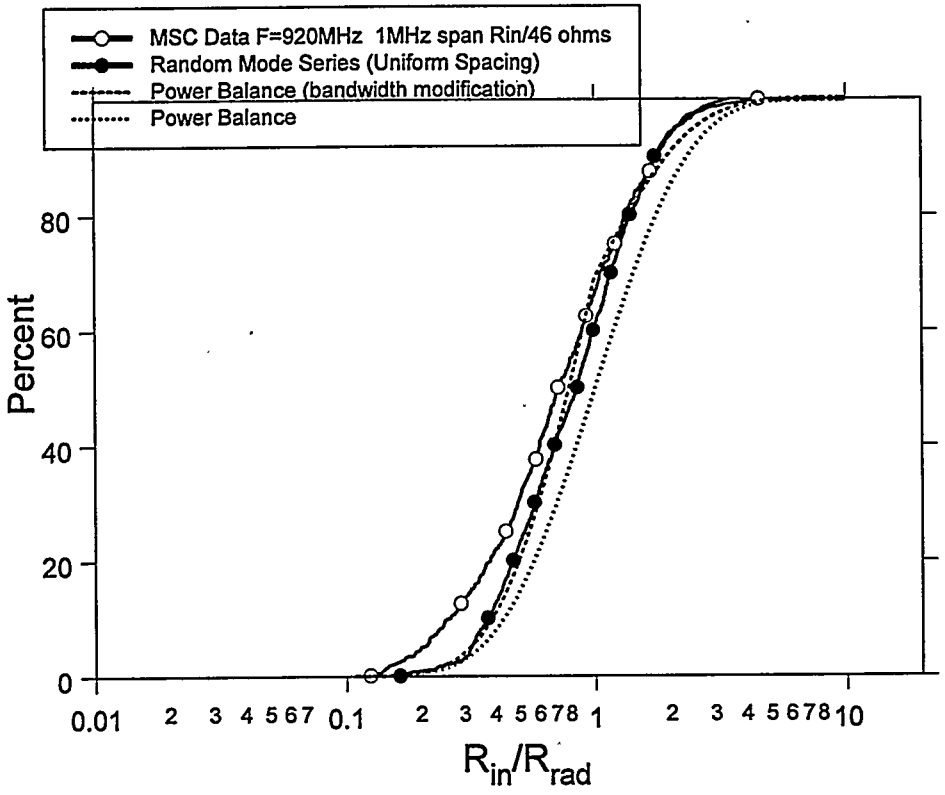


Figure 14: Normalized input resistance distribution from simulation, power balance (the bandwidth modification curve uses the asymmetric reflected field distribution) and experiment at 920 MHz.

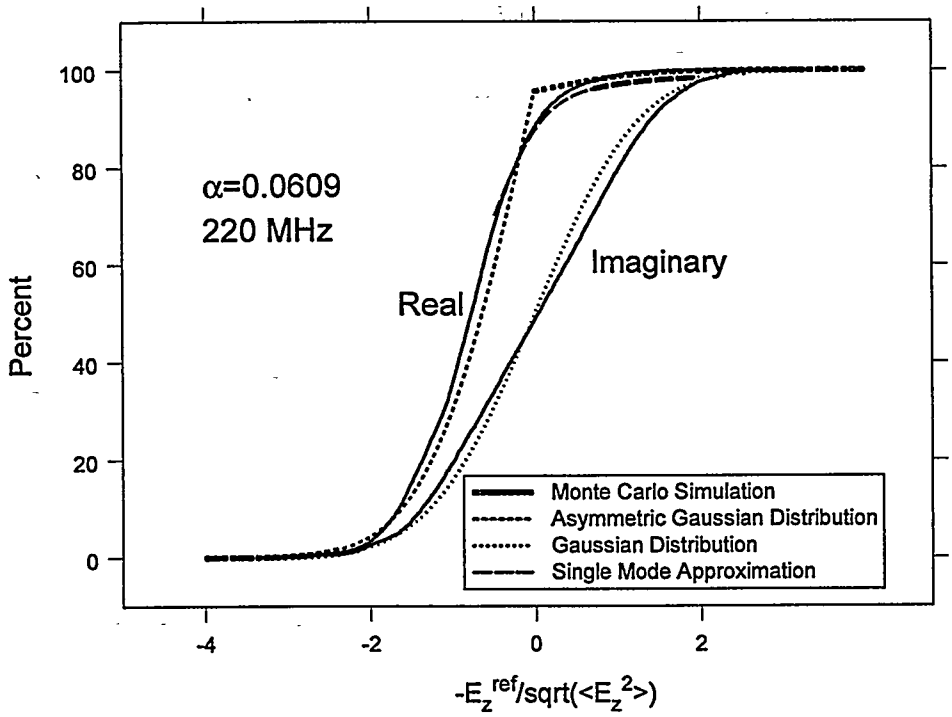


Figure 15: Normalized reflected field from simulation and simple fit at $\alpha \approx 0.0609$ (220 MHz).

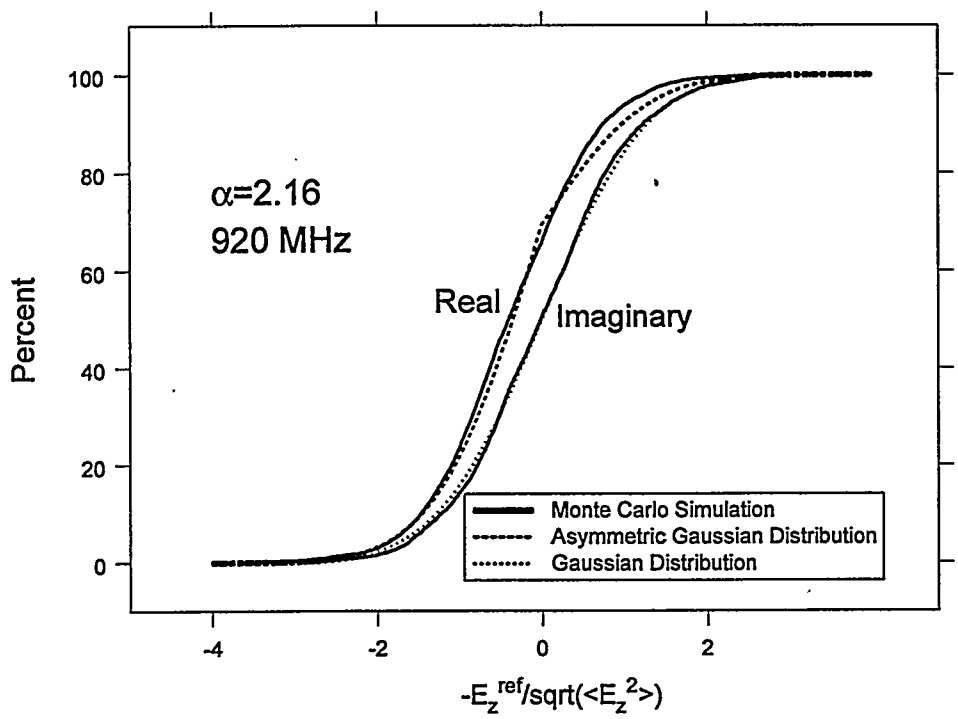


Figure 16: Normalized reflected field from simulation and simple fit at $\alpha \approx 2.16$ (920 MHz).